JOURNAL OF APPLIED CRYSTALLOGRAPHY
ISSN 1600-5767

Relationship between the volume of the unit cell of hexagonal-close-packed Ti, hardness and oxygen content after α-case formation in Ti–6Al–2Sn–4Zr–2Mo–0.1Si alloy

J. Baillieux, D. Poquillon* and B. Malard

CIRIMAT, Université de Toulouse, 4 allée E. Monso – BP 44362, Toulouse Cedex 04, 31030, France. *Correspondence e-mail: dominique.poquillon@inp-toulouse.fr

Received 13 June 2015
Accepted 30 November 2015

Edited by G. Kostorz, ETH Zurich, Switzerland

Keywords: titanium; oxygen diffusion; electron probe microanalysis; synchrotron radiation X-ray diffraction.

In this study, the influence of oxygen diffusion on the physical properties of Ti–6Al–2Sn–4Zr–2Mo–0.1Si was examined. Measurements were carried out directly on sample cross sections which were preoxidized at high temperature. The lattice parameter evolution was measured using synchrotron X-ray diffraction and was coupled with microhardness and electron probe micro-analyzer results with the aim of highlighting their relationships. The results show that the hardness and oxygen gradients along the oxygen diffusion zone in the alloy are similar to the evolution of the α-phase unit-cell volume quantified by X-ray diffraction. Linear relationships were found between these three parameters.

1. Introduction

Titanium and its alloys are attractive engineering materials in the aerospace industry because of their outstanding mechanical properties and excellent corrosion resistance. Ti–6Al–2Sn–4Zr–2Mo is commonly used in fan blades where the maximum temperature is in the range of 573–723 K (Lütjering & Williams, 2007). Another alloy, Ti–6Al–2Sn–4Zr–2Mo–0.1Si, is also used for manufacturing components where the temperature can be higher. At temperatures above 773 K and in oxygen-containing environments, these alloys oxidize rapidly. Between 873 and 973 K, the oxidation rate is parabolic; it then becomes linear with increasing temperature (Murray & Wriedt, 1987). Titanium has a high affinity to absorb oxygen when exposed to any oxidizing environment. This oxidation leads to the formation of an oxide layer (OL) on the surface with an oxygen diffusion zone (ODZ) in the metal, which is commonly called the α case (McReynolds & Tamirisakandala, 2011). The oxygen diffusion zone corresponds to the oxygen-enriched layer below the oxide layer due to oxidation.

In the 1960s, many authors studied the oxygen diffusion zone in titanium and tried to find what the oxygen maximum solubility was. In 1956, McQuillan & McQuillan (1956) announced that the oxygen maximum solubility in titanium could reach 50 at.%. One year later, Andersson *et al.* (1957) confirmed this value and added that the lattice parameters a and c were highly modified near the $TiO_{0.35}$ composition. Using X-ray diffraction (XRD) analysis, they suggested that oxygen atoms were randomly distributed in octahedral sites until 35 at.% content before becoming ordered. Above this content a new phase appears, the Ti_2O oxide. Finally, according to Kofstad (1988), the oxygen solubility is around

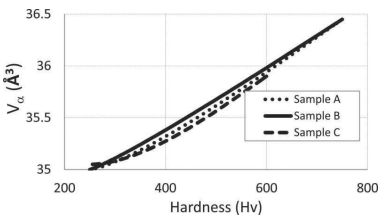

Table 1
Chemical composition of Ti–6Al–2Sn–4Zr–2Mo–0.1Si (Ti6242S) alloy (in at.%).

Ti	Al	Sn	Zr	Mo	Si	O
84.9–85.7	8.5–10.5	0.7–1.0	1.8–2.3	0.4–1.6	0.1–0.2	0.1–1.1

30 at.% in the α phase and 8 at.% for the β phase. These last values are quite similar to the oxygen solubility in a Zr alloy reported previously (Porte *et al.*, 1960).

The oxidation mechanism of titanium is complex owing to the high solubility of oxygen in the hexagonal-close-packed (h.c.p.) structure of α-titanium. A recent study showed that there are two other potential interstitial sites (hexahedral and crowdion) in α-Ti where the oxygen can be located (Wu & Trinkle, 2011). Oxygen is the most important interstitial solute in titanium alloys because the alloys' microstructural and mechanical properties are directly influenced by oxygen content (Liu & Welsch, 1988). Oxygen insertion modifies the lattice parameters of h.c.p. titanium, and a significant increase of the *c* parameter compared to the *a* parameter was observed using X-ray synchrotron measurements (Baillieux *et al.*, 2015). During oxidation, oxygen diffusion under the oxide scale leads to the development of an oxygen-enriched zone in the metal. The affected depth increases with increasing temperature and duration of exposure. This solid solution is harder and more brittle than the initial alloy. Because of this hardening effect, it is possible to characterize the affected zone using microhardness measurements (Göbel *et al.*, 2001; Guleryuz & Cimenoglu, 2009). Similarly, the gradient of oxygen content can also be measured using secondary ion mass spectrometry (SIMS) and electron probe microanalysis (EPMA) methods (McReynolds & Tamirisakandala, 2011; Poquillon *et al.*, 2013). Some authors have tried to establish a proportional link between the oxygen content, the lattice parameters and the microhardness (Murray & Wriedt, 1987). Dubertret (1970) concluded in his thesis that this proportional link was incorrect

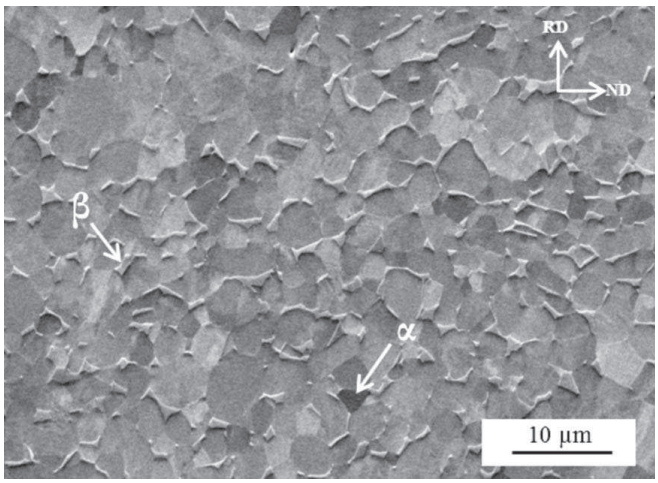

Figure 1
Microstructure of Ti–6Al–2Sn–4Zr–2Mo–0.1Si. Scanning electron microscopy observation with a forescatter detector, realized along the rolling (RD) and normal (ND) directions.

Table 2
Heat treatment conditions (sample, temperature and exposure duration).

Sample	A	B	C
Heat treatment	873 K, 1000 h	873 K, 2635 h	973 K, 170 h

and clearly confirmed that the hardness was not entirely linear with oxygen content for TiO_x (where $x \leq 0.7$). This fact is consistent with other results, as above 30 at.% of oxygen content a new ordered phase (Ti_2O) appears. In the present study, we focused on oxygen content below 30 at.%.

With the aim of finding the relationships between oxygen content, hardness and lattice parameters and using recent analysis methods such as X-ray synchrotron diffraction and EPMA, this study focuses on the titanium α phase below 30 at.% of oxygen content to avoid the new ordered phases. This kind of study has been realized on a commercially pure titanium alloy, Ti50A (Baillieux *et al.*, 2015), but not yet on an industrial alloy where the alloying elements can potentially modify the diffusion and consequently the relationships between the three parameters studied (Chaze & Coddet, 1987).

2. Material and methods

2.1. Material

Ti–6Al–2Sn–4Zr–2Mo–0.1Si is a near-α-titanium alloy used for its excellent creep resistance, good tensile strength, toughness and high thermal stability (Viswanathan, 2002). Its composition, which was determined by spectrographic analysis using standards for each element, is described in Table 1.

The addition of silicon in Ti6242S increases the creep resistance with silicide formation, which would inhibit the movement of mobile dislocations (Paton & Mahoney, 1976). This alloy was provided as a 1.6 mm-thick sheet after being hot and cold rolled and duplex annealed. The microstructure obtained, described in Fig. 1, is homogeneous with β-phase and α grains.

The microstructure was also studied using the EBSD technique using a JEOL field emission gun scanning electron microscope at 15 kV. The α grains are homogenous, with an average size close to 4 µm. The β volume fraction is around 11%.

2.2. Methods

Three parallelepiped samples [6 (rolling direction) × 4 × 1.6 mm] were cut from the sheet, polished using 600 grit SiC paper, and then cleaned in ethanol and acetone. Oxidations were performed at 873 and 973 K in a Carbolite furnace under laboratory air as described in Table 2.

Oxidation conditions were chosen according to a preliminary study on the oxidation and oxygen diffusion in the alloy (Baillieux, 2015). The aim of these oxidations is to develop an oxygen-enriched layer of about 50 µm for sample A and 70 µm for samples B and C. Then, to obtain a cross section of each sample, the two largest opposite faces (6 ×

4 mm) were polished after heat treatment to remove the oxide scale (OL) and the ODZ of these faces. At least 500 µm was removed to ensure proper measurements. Transverse observation enabled us to discriminate the different layers in each sample as shown in Fig. 2.

Microhardness profiles were realized on cross sections using a Buelher microhardness tester with a 10 g mass. The measurements were triplicated. The measuring error is close to 40 Hv for the mass used and increases for the low-hardness values. Three profiles of 15 indentations were realized on each sample to improve the measurement reliability. The observations and measurements of the resulting indent size were carried out with an optical microscope (Nikon MA 200).

With the aim of calculating the variation of lattice parameters in the oxygen diffusion zone, synchrotron X-ray measurements were performed on the ID11 beamline at the European Synchrotron Radiation Facility (ESRF) in Grenoble. The structural gradients were evaluated using a single-scan approach with a resolution of 2 µm using a FReLoN 4m (Kodak chip of 2048 × 2048 pixels with a channel size of 50 × 50 µm). The experimental method is similar to the protocol used for a previous study on pure titanium (Baillieux *et al.*, 2015). For the present experiment, the beam dimensions used were 300 µm width and 7 µm height. The step between each measurement was 2 µm. Calibrations of the wavelength and sample distances to the detector were performed using Si powder. The calculated error for the lattice parameters is lower than 0.01 Å. Analyses were triplicated for each sample along a line longer than the depth of the oxygen-enriched zone.

The sample positioning was carefully done to obtain a beam parallel to the top surface. Using a rotating sample holder, measurements were obtained at 0 and 180° to optimize sample positioning. After the data had been integrated on the entire two-dimensional diffractogram, the one-dimensional data were analyzed using the XRD software *DIFFRAC.SUITE TOPAS 4.2* (Bruker AXS, Karlsruhe, Germany). The two phases (α and β) were taken into account during the pattern matching process, and the software allows the calculation of the lattice parameters of each phase. The sample texture observed thanks to EBSD analysis was taken into account in the software. The lattice parameters of h.c.p. titanium were calculated and refined using a full-pattern-matching approach.

The oxygen content was studied using both SIMS and EPMA, but only EPMA can carry out a quantitative analysis of the oxygen content and is detailed below. Three EPMA profiles were performed along each sample using a CAMECA SXFive at 15 keV with a step measurement of 2 µm. The absolute error on the oxygen content is close to 0.1 at.%. The EPMA technique is a quite expensive method compared to microhardness measurement but allows a precise measurement of the oxygen content along the oxygen diffusion zone. Optical observations after the tint etching process were also used to evaluate the α case for Ti–6Al–4V. For the alloy of this study, the results were quite dependent on the sensitivity of the acid tint etch, and furthermore, the affected depth revealed always underestimated the oxygen diffusion zone compared to EPMA. It was particularly interesting to use this technique to check the ODZ depth measured by microhardness. The microhardness method is simple and cheap, but the precision of the ODZ depth depends also on the mass used for indentation. The EPMA method will give us the real oxygen profile, whereas XRD and hardness measurements indicate the effects of this oxygen ingress.

3. Results

Microhardness indentations were performed just behind the oxide layer and hardness profiles were plotted on graphs to determine the ODZ depth. The results for sample A are summarized in Fig. 3. Using a 10 g mass for indentation allows the hardness to be measured with a good resolution, but the values show a significant scatter in the bulk. The average hardness in the bulk was calculated and a fitted hardness profile was plotted. Then, the end of the ODZ corresponds to the point where the hardness is higher than 3% of the average hardness measured in the bulk of the alloy on the fitted profile. For sample A, this point corresponds to 50 µm behind the OL on the hardness profiles, so the ODZ depth is 50 µm.

The experimental hardness profiles are repeatable and confirm the hardness evolution in the ODZ. Thanks to the hardness gradient, it is possible to propose a hardness profile

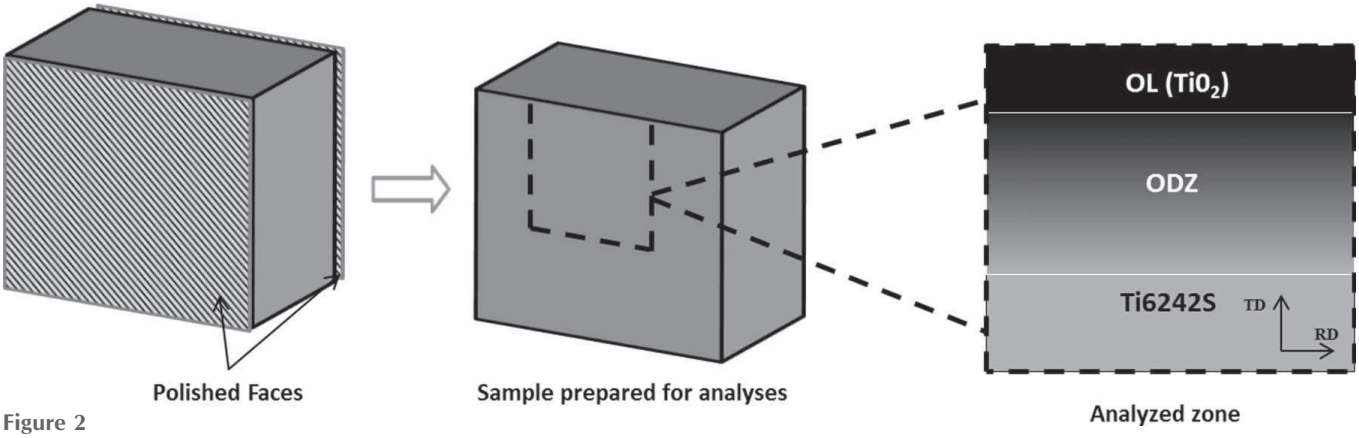

Figure 2
Sample preparation after oxidation and analyzed zone where measurements were performed.

Table 3
Oxygen diffusion zone depth (μm) measured using the microhardness method.

Sample	A	B	C
ODZ depth	50	70	68

using a diffusion model and particularly a simplification of Fick's second law (Kirkaldy & Young, 1987):

$$\frac{\partial C}{\partial t} = D\frac{\partial^2 C}{\partial x^2}, \tag{1}$$

where D is the constant of proportionality, termed the diffusion coefficient, and has units of square metres per second and C is the concentration. One solution for equation (1) in the case of diffusion of the gas phase in solids with semi-infinite thickness and constant surface concentration C_s of the gas is (Kirkaldy & Young, 1987)

$$\frac{C_x - C_0}{C_s - C_0} = 1 - \mathrm{erf}\left[\frac{x}{2(Dt)^{1/2}}\right], \tag{2}$$

where C_x is the concentration of the diffused atoms at distance x after time t, C_0 is the initial concentration in the bulk of the metal at time t_0, and the expression $\mathrm{erf}\{x/[2(Dt)^{1/2}]\}$ is the Gaussian error function, whose values can be extracted from mathematical tables for different $x/[2(Dt)^{1/2}]$ values. Equation (2) can be adapted to propose a hardness profile replacing the gas concentration C_x with Hv_x (the hardness at distance x). The equation becomes

$$\mathrm{Hv}_x = \mathrm{Hv}_{\min} + (\mathrm{Hv}_{\max} - \mathrm{Hv}_{\min})\,\mathrm{erfc}\left[\frac{x}{2(Dt)^{1/2}}\right], \tag{3}$$

erfc being the complementary error function. Using equation (3), it was possible to plot in Fig. 3 the hardness profile that fits the experimental profiles and to determine the value of D. The other hardness profile graphs for samples B and C allowed us to determine the ODZ depth and the D constant for each oxidation temperature studied. The ODZ depth results measured with the microhardness method are summarized in Table 3, and the values for B and C are similar, as expected for this study.

Oxygen content profiles resulting from EPMA allowed us to determine the ODZ depth. The results for sample A are summarized in Fig. 4. Three oxygen profiles were measured. The results are repeatable and define an ODZ depth of 48 μm, which is close to the value measured by the microhardness method (50 μm). Equation (2) can again be used to fit the oxygen content profile. The equation becomes

$$[\mathrm{O}]_x = [\mathrm{O}]_{\min} + ([\mathrm{O}]_{\max} - [\mathrm{O}]_{\min})\,\mathrm{erfc}\left[\frac{x}{2(Dt)^{1/2}}\right]. \tag{4}$$

The oxygen profile fitted using this equation is plotted in Fig. 4. The measured depth of the oxygen-enriched zone was 69 μm for sample B and 67 μm for sample C.

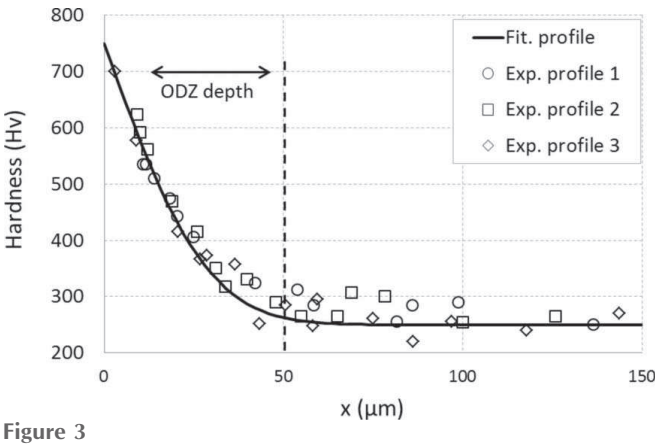

Figure 3
Experimental microhardness profiles for sample A (873 K, 1000 h) and corresponding fitted profile.

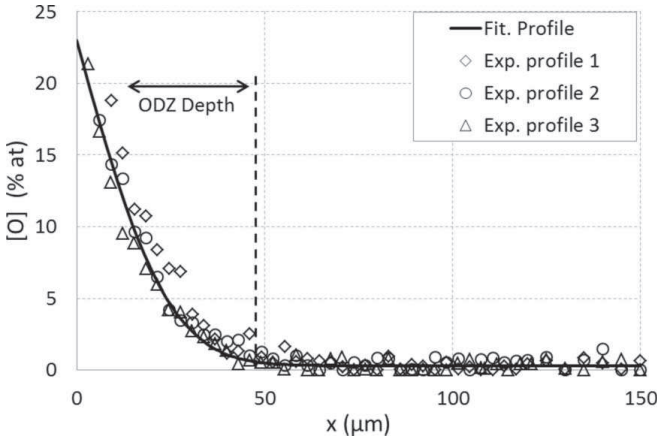

Figure 4
Experimental oxygen profiles (using EPMA) for sample A (873 K, 1000 h) and corresponding fitted profile.

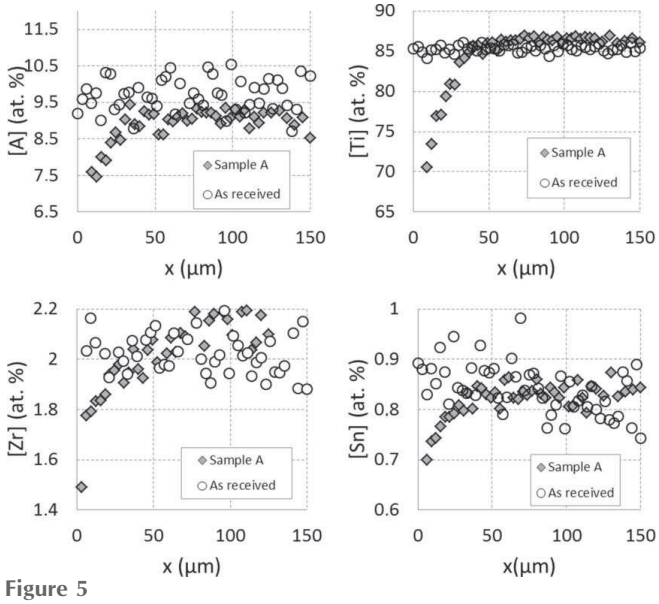

Figure 5
Main element content profiles measured for sample A behind the oxide layer along the ODZ and for the as-received sample using EPMA.

The main elements that compose Ti–6Al–2Sn–4Zr–2Mo–0.1Si were analyzed along the ODZ with the aim of observing a potential effect of the oxygen diffusion. Their content profiles for sample A are summarized in Fig. 5. Beginning from the oxide layer, the profiles for sample A show an increase of [Al], [Ti], [Zr] and [Sn] until a stabilized level is reached near to 50 µm behind the oxide layer. For [Si] and [Mo], no modifications were observed along the ODZ. An as-received sample (without the ODZ) was also analyzed to compare the stabilized level of element content in the bulk. The results show that the stabilized level of [Al], [Ti], [Zr] and [Sn] after the ODZ for sample A is comparable to the [Al], [Ti], [Zr] and [Sn] contents measured on the sample as received.

The last parameters measured were the lattice parameters a and c of α-titanium. The β-phase parameters were also measured, but the evolution was more significant for the α phase. The resulting α-phase unit-cell volume profiles for sample A are summarized in Fig. 6. As for the microhardness and EPMA profiles, the α-phase unit-cell volume profiles defined a measurable ODZ. The ODZ depths measured with synchrotron X-ray measurements are 48 µm for sample A, as observed in Fig. 6, 68 µm for sample B and 67 µm for sample C.

To define a fitted profile, equation (2) becomes

$$[V\alpha]_x = [V\alpha]_{\min} + ([V\alpha]_{\max} - [V\alpha]_{\min})\,\mathrm{erfc}\left[\frac{x}{2(Dt)^{1/2}}\right]. \quad (5)$$

The fitted profile plotted in Fig. 6 is in good agreement with the three experimental profiles.

4. Discussion

For the three tested conditions, the oxygen content, the α-phase unit-cell volume and the hardness decrease from the metal/oxide interface to the bulk. The limit of the oxygen diffusion zone is shown with the three methods used. Moreover, the ODZ depths measured for each method are nearly equal. This confirms that these gradients are directly linked to the oxygen diffusion and insertion in α-titanium, which affect the lattice parameters and hardness because of interactions between interstitial oxygen and dislocations.

Similar oxygen diffusion depths (around 70 µm) are measured for samples B and C, which were oxidized at different temperatures. The temperature/exposure time equivalence allowed the development of an ODZ of comparable depth, but all three of the parameters studied were higher at the oxide/metal interface for sample B oxidized at 873 K. A thicker oxide scale was observed for sample C oxidized at 973 K. Just under the oxide scale, the oxygen content was 24 at.% for sample B and 15 at.% for sample C. These results confirm that, even if it is possible to develop the same ODZ depths at different temperatures, the oxidation temperature affects the diffusion and particularly the oxygen content at the oxide/metal interface owing to the different thermodynamic equilibrium at the metal/oxide interface. This fact can be explained because the oxide layers formed were different. In general the oxide grain size increases with increasing temperature, and accordingly the oxide crystallites are larger and better developed than at lower temperature (Kofstad *et al.*, 1961; Kofstad, 1967). Because the oxide layer formed on sample C is thicker than that on sample B, the contribution due to oxygen dissolution in the oxygen diffusion zone for sample C is smaller than the contribution for sample B (Hurlen, 1961; Gaddam *et al.*, 2015). In addition, this diminution of oxygen content at the oxide/metal interface for sample C can be influenced by oxygen diffusion in the oxide scale (rutile).

Fig. 5 illustrates the alloying element contents in the ODZ and it confirms that an oxygen gradient affects the alloying elements, particularly those that are dissolved in the α phase as Al, Sn and Zr. At the end of the ODZ, the alloying element contents are not modified anymore and correspond to the initial alloy composition. It is important to note that oxygen diffusion only perturbs the alloy composition along the ODZ and does not affect the alloy elsewhere. For the elements that are not dissolved in the α phase as Si and Mo, their contents are not modified as the other elements and remain unchanged along the ODZ. This observation can be explained because, as mentioned before, the oxygen solubility is higher in the α

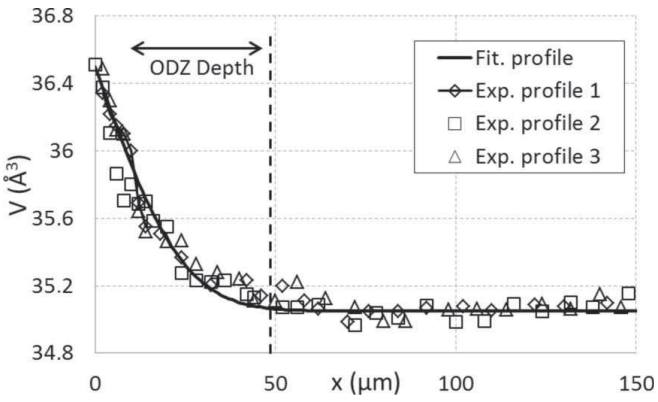

Figure 6
Experimental α-phase unit-cell volume profiles for sample A (873 K, 1000 h) and the corresponding calculated α-phase unit-cell volume profile.

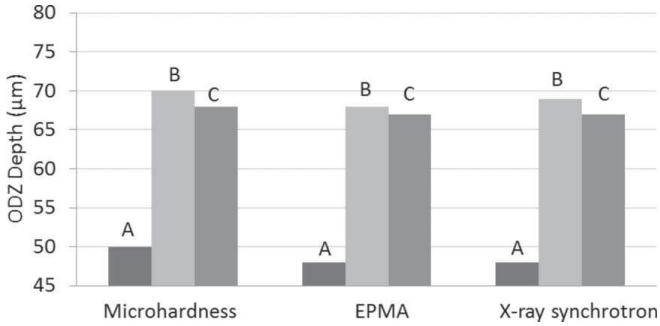

Figure 7
ODZ depths measured for samples A, B and C using the three experimental methods.

Table 4
Diffusion coefficients ($m^2\ s^{-1}$) identified for samples A, B and C using the three experimental methods.

Analysis method	Sample A	Sample B	Sample C
Microhardness method	7×10^{-17}	7×10^{-17}	1×10^{-15}
EPMA method	6×10^{-17}	5×10^{-17}	7×10^{-16}
Synchrotron X-ray measurements	5×10^{-17}	6×10^{-17}	5×10^{-16}

phase compared to the solubility in the β phase (Kofstad, 1988).

The ODZ depths are summarized in Fig. 7 and confirm that the three methods find similar affected depths for each sample. Using three different methods, the ODZ depths were clearly determined and, thanks to the adaptation of Fick's second law [equation (2)], fitted profiles were plotted for each experiment. It was possible to calculate a diffusion coefficient D for each sample and each method.

These D coefficients are summarized in Table 4. The diffusion coefficient is temperature dependent. For samples A and B, both oxidized at 873 K, all the coefficients calculated with the three methods are comparable. For sample C, oxidized at 973 K, again the D coefficients are comparable for the three methods, but they are higher than the coefficients calculated for samples A and B, in accordance with the parabolic oxidation kinetics.

The coefficients obtained are in good agreement with the literature (Liu & Welsch, 1988; Mishin & Herzig, 2000). Even though we only have the value of D for two temperatures, the activation energy could be estimated for each method, and these values are compared with the literature in Table 5.

The experimental methods used (microhardness, EPMA and X-ray synchrotron diffraction) to determinate the activation energies for the diffusivity in titanium allow us to find values in good agreement with values available in the literature. Table 5 shows also that an inexpensive method such as microhardness is a good choice to determine the activation energies. Furthermore, if previous studies of lattice parameters and oxygen content have been performed like in the present work, it is then possible to define these parameters knowing just the local hardness along the oxygen diffusion zone.

Finally, according to the coefficients calculated and the extrema of the parameters measured for each experiment it was possible to highlight the relationships between oxygen content, microhardness and α-phase unit-cell volume. Figs. 8–10 summarize these relationships.

The maximum oxygen content measured was below 25 at.% and no ordered phase like Ti_2O was formed. In the range of [0–25 at.%], the three graphs clearly confirm a proportional relationship between the three parameters studied. Note that even for sample C, where the maximal oxygen content did not reach 15 at.%, the proportional relationship is in good agreement with the relationship calculated for samples A and B where oxygen maximum content was close to 25 at.%.

The relationships observed seem linear, in accordance with the idea that oxygen atoms are randomly distributed in octa-

Table 5
Activation energies for the diffusivity of oxygen in titanium.

Alloy	Method	Activation energy ($kJ\ mol^{-1}$)	Reference
Ti6242S	Microhardness	188	This work
Ti6242S	EPMA	175	This work
Ti6242S	X-ray synchrotron	163	This work
Ti–6Al–4V	SIMS	156	Poquillon *et al.* (2013)
CP–Ti	Microhardness	186	Broumas *et al.* (2003)
Ti–0.2 at.% O	Internal friction	188	Gupta & Weinig (1962)
Ti–3.5 at.% O	Internal friction	201	Pratt *et al.* (1954)
Ti75A	Microhardness	140	Roe *et al.* (1960)
CP–Ti	Microhardness	203	Rosa (1970)
		150	Revyakin (1961)
Tracer diffusivity			
α-Ti[44]	Tracer	173	Dyment & Libanati (1968)

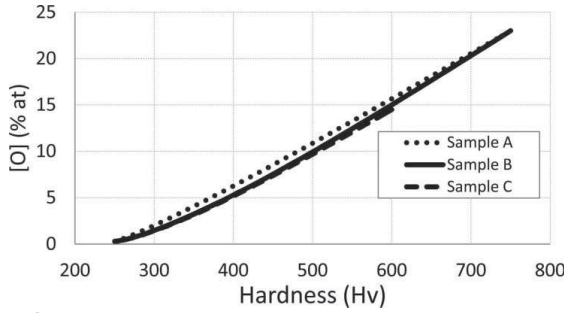

Figure 8
Oxygen content as a function of microhardness for samples A, B and C, based on the fitted profiles using experimental data.

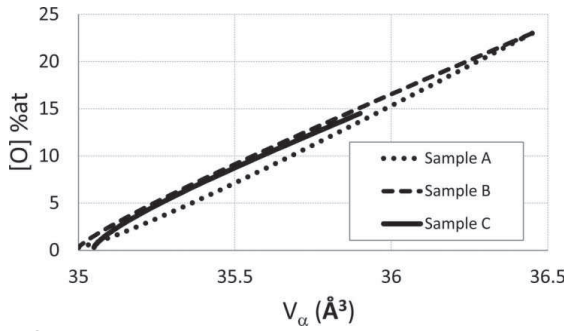

Figure 9
Oxygen content as a function of α-phase unit-cell volume (V_α) for samples A, B and C, based on the fitted profiles using experimental data.

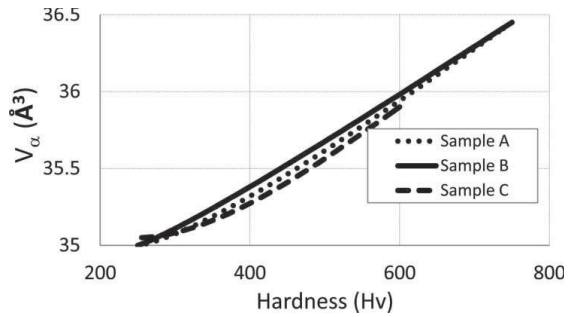

Figure 10
α-phase unit-cell volume (V_α) as a function of microhardness for samples A, B and C, based on the fitted profiles using experimental data.

hedral sites of h.c.p. titanium. It appears that the linear link is more difficult to observe for the low oxygen content, but this observation can be explained by the fact that microhardness is difficult to measure below 2 at.% of oxygen owing to the precision of the equipment.

5. Conclusion

Comparisons between hardness, oxygen content and lattice parameter evolution after α-case formation at 873 and 973 K in Ti–6Al–2Sn–4Zr–2Mo–0.1Si alloy were highlighted. The conclusions from the present study are as follows:

(1) The ODZ depth is predictable for both temperatures studied and can be determined with the three methods used in this present work.

(2) An oxygen gradient affects the alloying elements and particularly Al, Sn and Zr dissolved in the α phase. The oxygen diffusion only perturbs the alloy composition along the ODZ and does not affect the alloy once the ODZ is achieved.

(3) The maximum oxygen content measured below the oxide layer is temperature dependent.

(4) The diffusion coefficients calculated with the three methods are similar and the activation energies for the diffusivity of oxygen are in good agreement with the literature.

(5) Thanks to the adaptation of Fick's second law, it was possible to determine mathematical profiles of the gradient observed for each experiment. Linear relationships were obtained between hardness, oxygen content and α-phase unit-cell volume in the absence of the ordered phase Ti_2O.

Acknowledgements

The authors gratefully acknowledge Jonathan Wright from beamline ID11 at the ESRF for his help with synchrotron measurements, Sophie Gouy and Philipe de Parseval from the Centre de Micro Caractérization Raymond Castaing for the EPMA analysis, and Teresa Hungria for the SIMS measurements.